DNA Bending by Charged Peptides: Electrophoretic and Spectroscopic Analyses†

Robert J. McDonald,‡,§ Anatoly I. Dragan,|| William R. Kirk,§ Kevin L. Neff,⊥ Peter L. Privalov,|| and L. James Maher, III*,⊥

Medical Scientist Training Program, Department of Molecular Pharmacology and Experimental Therapeutics, and Department of Biochemistry and Molecular Biology, Mayo Clinic College of Medicine, Rochester, Minnesota 55905, and Department of Biology, Johns Hopkins University, Mudd Hall, 3400 North Charles Street, Baltimore, Maryland 21218

Received September 15, 2006; Revised Manuscript Received December 12, 2006

ABSTRACT: We are testing the idea that placement of fixed charges near one face of the DNA double helix can induce DNA bending by a purely electrostatic mechanism. If stretching forces between DNA phosphates are significant, fixed charges should induce DNA bending by asymmetrically modulating these forces. We have previously tested this hypothesis by adding charged residues to small bZIP DNA binding peptides and monitoring DNA bending using electrophoretic phasing assays. Our results were consistent with an electrostatic model of DNA bending in predicted directions. We now confirm these observations with fluorescence resonance energy transfer (FRET). Using a "U"-shaped DNA probe, we report that DNA bending by charged bZIP peptides is readily detected by FRET. We further show that charged bZIP peptides cause DNA bending rather than DNA twisting.

DNA bending plays a central role in many biological processes such as nucleosome compaction, transcription activation, and recombination (*1*−*3*). The bending persistence length (*p*) of naked double-stranded DNA is ∼150 bp under physiological conditions. DNA molecules much longer than *p* will spontaneously collapse to an average end-to-end distance that is related to the DNA contour length (*L*) by $\sim(pL)^{1/2}$ (*4*). For example, a DNA molecule of 3×10^9 bp (∼1 m) will adopt conformations with an average end-to-end distance of ∼400 μm in physiological buffer [a spontaneous compaction of 2500-fold (*4*−*6*)]. In contrast, segments of DNA on the length scale of *p* are relatively rigid, with an average spontaneous axial deflection of only one radian. The local rigidity of DNA must be overcome for biological function. Structural studies of DNA bending proteins such as CAP (*7*, *8*), the histone octamer (*1*, *9*), and HMG proteins (*10*, *11*) have suggested an important role for electrostatics in protein-mediated DNA bending (*12*). We have been measuring DNA bending after creating laterally asymmetric charge distributions along DNA (*13*−*16*) in order to determine the extent to which electrostatic forces can modify the shape of DNA.

Our previous experimental results are consistent with the premise that phosphate repulsions along the backbone of the double helix contribute to the observed rigidity of DNA. Manning's counterion condensation model makes quantitative predictions about high local concentrations of cations attracted to a densely charged polyelectrolyte such as DNA (*17*, *18*). The resulting counterion cloud partially reduces interphosphate repulsions through charge neutralization. Such radially uniform charge neutralization is predicted to increase DNA flexibility, an effect that has been observed when DNA stiffness is measured by optical tweezers in the presence of counterions of higher valence (*19*). Free cations are believed to loosely interact with the surface of DNA, though there is evidence for sequence-specific accumulation of cations influencing the geometry of the DNA grooves (*20*−*25*). More dramatically, sequence-specific DNA binding proteins can position charges near one face of the DNA helix forming long-lived electrostatic interactions. Such laterally asymmetric charge distributions should generate bending forces by local reduction (cations) or enhancement (anions) of interphosphate repulsions (*12*, *26*−*28*). According to this model, the asymmetric reduction or enhancement of electrostatic repulsive forces on one DNA face causes DNA bending by unbalancing the repulsive forces on the two sides of the double helix.

Transcription factor Gcn4p of *Saccharomyces cerevisiae* regulates amino acid biosynthesis during the GCN response to nutrient starvation (*29*, *30*). Gcn4p binds as a homodimer to both AP1 (5′-ATGACTCAT) and CRE (5′-ATGACGTCAT) sequences (*31*) through the carboxy-terminal basic leucine zipper (bZIP) domain (60 amino acids) of the protein. The bZIP domain has been intensely studied as a biophysical model because of its simple secondary structure and prevalence [found in over 50 eukaryotic transcription factors including mammalian oncogenes Fos and Jun (*32*, *33*)]. Debate over the ability of Jun and Fos dimeric bZIP peptides to bend DNA originated from conflicting results obtained using different peptides in electrophoretic, cyclization, and minicircle assays (*34*−*40*). Interestingly, bZIP·DNA cocrystals of the CRE site suggest that Gcn4p peptides do not

† Supported by the Mayo Foundation, NIH Grants GM 054411 and GM 75965 to L.J.M., and NSF Grant MCB 0519381 to P.L.P.

* To whom correspondence should be addressed. Tel: 507-284-9041. Fax: 507-284-2053. E-mail: maher@mayo.edu.

‡ Medical Scientist Training Program, Mayo Clinic College of Medicine.

§ Department of Molecular Pharmacology and Experimental Therapeutics, Mayo Clinic College of Medicine.

|| Department of Biology, Johns Hopkins University.

⊥ Department of Biochemistry and Molecular Biology, Mayo Clinic College of Medicine.

10.1021/bi061921a CCC: $37.00
Published on Web 02/06/2007

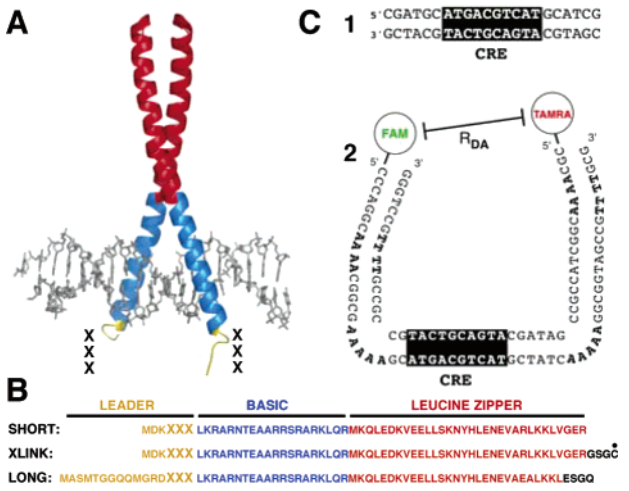

FIGURE 1: Experimental design. (A) Gcn4p bZIP homodimer bound to the CRE DNA sequence (*41*). The leucine zipper (red) and basic (blue) domains are indicated. Charge variants (XXX) of bZIP peptides were created near the N-terminus (gold) by mutation of the wild-type sequence (PAA, neutral) to either anionic (EEE) or cationic (KKK) forms. (B) bZIP-XXX peptide scaffolds studied. The indicated cysteine residue (dot) allowed oxidation to a cross-linked covalent homodimer form. Color coding is as in panel A. (C) DNA duplexes **1** and **2** contained either a CRE site (shown) or an AP1 site (5′-ATGACTCAT).

significantly bend the CRE site (*41*−*44*). The intent of the present study is not to resolve this prior controversy. Rather, the focus here is to use a homodimeric yeast bZIP domain as a scaffold to position charged residues near DNA for testing electrostatic effects in DNA bending [Figure 1A (*14*, *15*)].

Electrophoretic phasing assays are sensitive to DNA bending because mobility in native gels is exquisitely dependent upon DNA shape (*45*, *46*). We have previously used electrophoretic phasing assays to test DNA bending by charge variants of bZIP or basic helix−loop−helix (bHLH) domains (*13*, *15*, *47*). Bending interpretations in electrophoretic phasing assays involving native and charge-modified bZIP peptides are subject to the assumption that no phase-dependent mobility changes arise from the shape, flexibility, and/or gel-matrix interactions of the elongated peptide (*34*, *36*, *39*, *40*). We previously controlled for such possibilities by showing that charge-induced DNA bending persisted after appending globular domains to bZIP peptides (*48*) and with the less elongated bHLH domain as a charge scaffold (*47*).

To independently confirm the role of electrostatics in DNA bending by charged peptides, we now apply fluorescence resonance energy transfer (FRET), a useful spectroscopic approach to measure macromolecular distances from 10 to 100 Å (*49*, *50*). We previously applied FRET analysis to bZIP charge variants bound to linear DNA, showing results consistent with DNA bending (*13*). We now present studies using a more sensitive "U"-shaped DNA duplex that allows estimation of both the magnitude and direction of small DNA bends that are difficult to observe in linear DNA (*51*, *52*). We demonstrate DNA bending in opposite directions by cationic and anionic bZIP charge variants. These results compare favorably with DNA bending estimates obtained by electrophoretic phasing experiments, suggesting a significant role for electrostatics in DNA rigidity and bending.

MATERIALS AND METHODS

Plasmids. Gcn4p expression plasmid pJ951, derived from pET3a (Novagen), encodes the 57 amino acid $bZIP_{SHORT}$ domain of Gcn4p and was generously provided by T. Ellenberger (*53*). Plasmid pJ013, a derivative of a pET3b (Novagen), encodes 67 amino acids of the $bZIP_{LONG}$ peptide Gcn4p and was generously provided by B. Müller-Hill (*31*). A Gcn4p variant containing a disulfide cross-link, $bZIP_{XLINK}$, was prepared by chemical oxidation of a peptide encoded by a plasmid generated through site-directed mutagenesis of pJ951. Charge variants of all three peptide scaffolds ($bZIP_{SHORT}$, $bZIP_{XLINK}$, $bZIP_{LONG}$) were then generated by site-directed mutagenesis of the wild-type sequence PAA (XXX, Figure 1A,B) to create anionic (EEE) and cationic (KKK) forms. Three charge variants were generated for each of three peptide scaffolds to create nine expression plasmids. CRE-containing derivatives of plasmids pDP-AP-1−21, −23, −25, −26, −28, −30 (*43*) were created by mutagenic insertion of a single G·C base pair into the AP1 sequence (5′-ATGACTCAT) to create the CRE sequence (5′-ATGACGTCAT) for DNA duplexes used in electrophoretic phasing analysis.

Oligonucleotides. HPLC-purified, dye-conjugated oligonucleotides used for the generation of U-shaped FRET duplexes (Figure 1C) were purchased from Integrated DNA Technologies, Inc. FAM and TAMRA dyes were linked to each oligonucleotide via a 5′-phosphodiester bond, hexamethylene linker, and amide bond at the dye. Unmodified oligonucleotides were purified by denaturing polyacrylamide gel electrophoresis followed by reverse-phase column purification and desalting (Sep-Pak; Waters Corp.).

Protein Expression and Purification. Gcn4p bZIP variants were expressed from BL21(DE3) cells carrying the auxiliary pLysS plasmid in LB media (*53*). After induction and harvesting, cells were lysed using a combination of sonication and pneumatic sheering with an Avestin Emulsiflex-C5 disruptor (140 psi, 4 °C). Crude cell lysates were clarified by centrifugation (20000*g*, 45 min, 4 °C) followed by heating at 70 °C for 15 min to denature and precipitate contaminating proteins. Clarified lysates were treated with 0.3−0.5% (w/v) polyethylenimine (Sigma) for 30 min at 4 °C while slowly stirring to precipitate sheared bacterial DNA fragments. The resulting lysate was concentrated using a 5000 molecular weight cutoff centrifugal concentrator (VivaSpin 20; VivaScience) before final purification by C_{18} reverse-phase HPLC [C_{18} preparative reverse-phase column (250 × 21.2 mm), Beckman 127P System Gold; buffer I, 0.1% trifluoroacetic acid (TFA); buffer II, 80% CH_3CN, 0.1% TFA, gradient of 10%−70% buffer II over 50 min]. Peptide purity was assessed by ESI GC-MS to be >95%. Purified peptides were lyophilized for long-term storage. To examine the effects of solution conditions, three buffer systems were used in the subsequent assays (buffer A, 10 mM K/HPO_4, pH 6.2, 100 mM KCl; buffer B, 10 mM Na/HPO_4, pH 7.4, 137 mM NaCl, 2.7 mM KCl, 5% glycerol, 0.025% NP-40; buffer C, 50 mM Tris−H_3BO_3, pH 8.3, 1 mM EDTA).

Circular Dichroism Spectroscopy. CD spectra were recorded using a Jasco 810 spectropolarimeter. Far-UV CD spectra were obtained in the continuous mode, collecting measurements every 1 nm with an averaging time of 5 s at 295 K between 260 and 200 nm. Protein samples were 10 μM in 0.2 cm path length cells. Spectra were acquired in

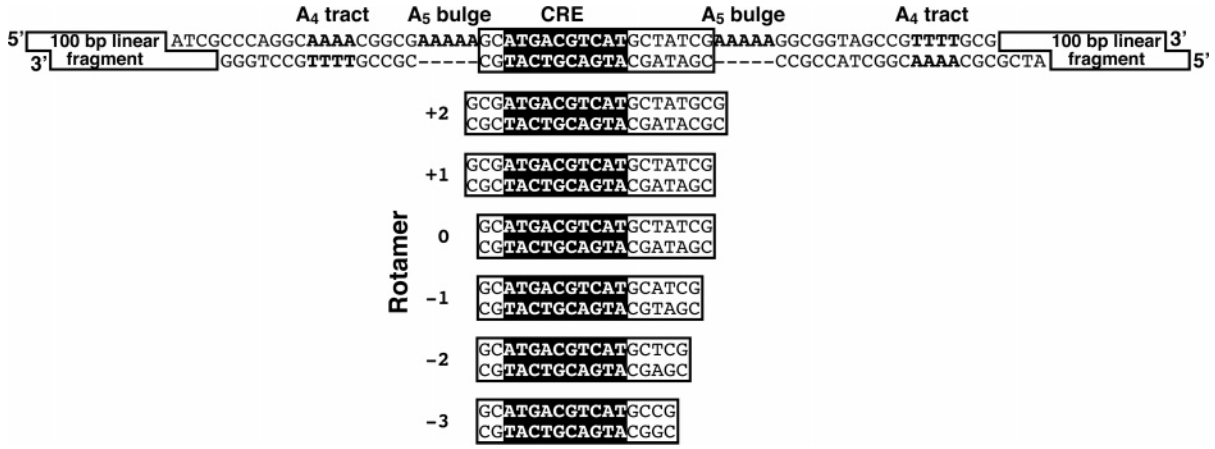

FIGURE 2: Rotamer design. Rotamer derivatives of **2** generated by the addition or deletion of a single bp flanking the CRE binding site. The sequence alterations of the rotamer derivatives (−**3**, −**2**, −**1**, **0**, +**1**, +**2**) are shown. Zero (**0**) refers to the unlabeled form of FRET probe **2**. ~100 bp linear DNA fragments were then ligated to the arms of the rotamers for gel electrophoresis studies.

buffer B with either 10 μM bZIP peptide or a complex of bZIP·**1** at a final molar ratio of 1:1.1. All baseline buffer and nucleic acid contributions to ellipticity were subtracted after spectral collection. α-Helical estimates of bZIP peptides from CD data are based upon previously published equations (*54*).

Binding Affinity Measurements. CRE duplex **1** (Figure 1C) was radiolabeled using [α-^{32}P]dNTPs and the Klenow fragment of *Escherichia coli* DNA polymerase I. Nonfluorescent U-shaped duplex **2** (Figure 1C) was radiolabeled using [γ-^{32}P]ATP and polynucleotide kinase (New England Biolabs). Radiolabeled duplexes were purified from unincorporated nucleotides by size-exclusion chromatography using spin columns (Chromaspin TE-10; Clontech). bZIP sample concentrations were determined as described (*55*) and then diluted into buffer B. Binding reactions were performed with peptide dilutions (10 pM−1 μM) incubated with radiolabeled DNA duplexes (**1**, 50 pM; **2**, 50 nM) in final reaction volumes of 20 μL containing buffer B supplemented with 100 μg/mL bovine serum albumin (BSA). Binding reactions were incubated on ice for 30 min before separation by native 8% polyacrylamide gel electrophoresis (29:1 acrylamide:bisacrylamide) in 0.5× TBE buffer for 750 V·h at 22 °C. Dried gels were analyzed by storage phosphor technology using a STORM 840 scanner (Amersham). Equilibrium dissociation constant (K_d) values of bZIP peptides (P) for the DNA duplex (D) were estimated by measuring the fractional occupancy (θ) of the radiolabeled duplex as a function of the bZIP concentration according to

$$\theta = \{([D]_{total} + K_d + [P]_{total}) - \sqrt{([D]_{total} + K_d + [P]_{total})^2 - 4([D]_{total}[P]_{total})}\}/2[D]_{total} \quad (1)$$

Data were fit using nonlinear least-squares analysis for K_d estimates using Kaleidagraph software.

Electrophoretic Phasing Assays of DNA Binding. Five DNA duplexes for phasing analyses were generated and radiolabeled by polymerase chain reaction (PCR) from CRE derivatives of pDP-AP-1-XX plasmids (*43*). DNA duplexes were incubated on ice for 30 min with sufficient peptide for ~50% mobility shift in buffer B or C and 100 μg/mL BSA before separation using native 8% polyacrylamide gel electrophoresis (29:1 acrylamide:bisacrylamide) in 0.5× TBE buffer for 2000 V·h at 22 °C. Electrophoretic phasing analysis and calculations were performed as previously described (*56*).

Rotamer Generation and Analysis. Single bp additions and deletions adjacent to the CRE sequence were made to generate six rotamer derivatives of **2** (+**2**, +**1**, **0**, −**1**, −**2**, −**3**), where rotamer **0** has the same twist geometry as FRET probe **2**. After annealing, ~100 bp linear DNA fragments with compatible cohesive ends (*56*) were incubated with rotamers in the presence of T4 DNA ligase (4 units/20 μL ligation reaction; New England Biolabs) to extend the rotamers in order to enhance shape detection by electrophoresis (Figure 2). Extended rotomers were radiolabeled using [α-^{32}P]dNTPs and the large fragment of *E. coli* polymerase I (New England Biolabs). Radiolabeled duplexes were purified from unincorporated nucleotides by size-exclusion chromatography using spin columns (Chromaspin TE-10; Clontech). Radiolabeled extended rotamers were incubated with $bZIP_{LONG}$ charge variants in 20 μL reactions containing binding buffer B supplemented with 100 μg/mL bovine serum albumin (BSA). Free and bZIP bound rotamer probes were resolved using native 4.5% polyacrylamide gel electrophoresis (29:1 acrylamide:bisacrylamide) in 0.5× TBE buffer for 1200 V·h at 22 °C. Normalized mobilities of each set of rotamer probes were plotted against bp spacing and fit to a cosine function:

$$\mu_{rel} = a\cos(bx - c) + d \quad (2)$$

where a is amplitude, b is frequency, c is phase shift, and d is vertical offset of the cosine function. Fits showed similar minima of the cosine functions identifying the intrinsic twist in FRET probe **2** (rotamer **0**).

Modeling of the U-Shaped FRET Probe. The nonplanarity of **2** required a model to account for both the inherent twist (ϕ) and induced bend (β) of the CRE/AP1 site. Twist and bend at the base of the U are represented by two transformations in this model (Figure 3A). Holding half of the model fixed, the change in the end-to-end distance between the donor and acceptor due to both twisting and bending is estimated as follows. The donor (green) and acceptor (red) occupy points p_1 (x,y,z) and p_2 (x',y',z'), respectively. Point p_2 can be moved to point p_3 while holding p_1 stationary, and

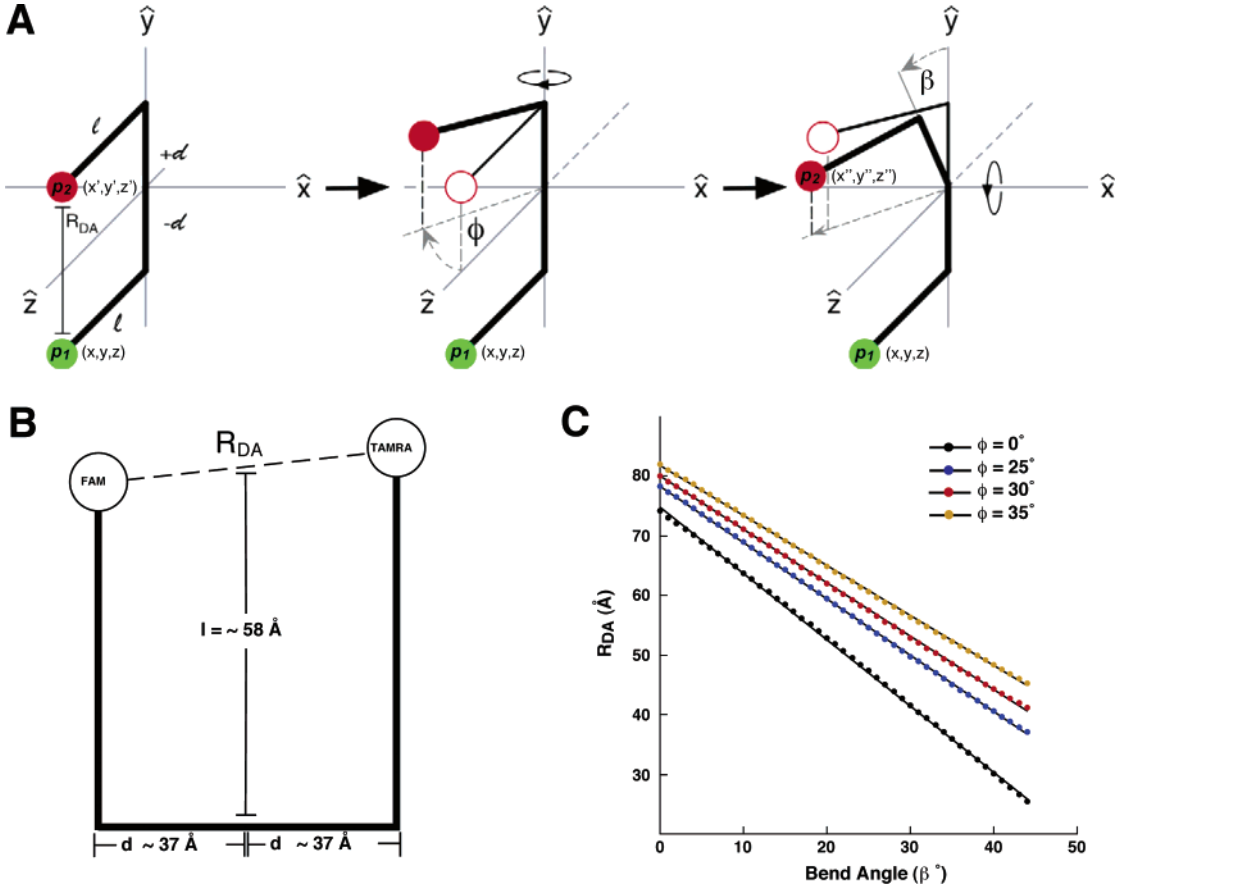

FIGURE 3: Geometric model of U-shaped FRET probe **2**. (A) Transformations of **2** include twisting about the *y*-axis resulting in nonplanarity shown by the angle ϕ (first transformation) and bending in the center of the CRE site (about the *x*-axis) by the angle β (second transformation). (B) Planar model based on **2** and previous experimental data (*42*). Distance *d* is estimated to be 37 Å from electrophoretic data (Figure 7), suggesting that the measured donor−acceptor distance of 80 Å includes a 30° twist in the U-shaped probe. (C) Relative insensitivity of the end-to-end distance (R_{DA}) and derived bend angle (β) on twist parameter (ϕ) for values near the actual twist estimate of 30°. Calculated values are depicted as filled circles with linear fits.

this movement of p_2 to (x'',y'',z'') vis-à-vis a twist and bend of the CRE site can be defined by matrix ***R*** (*57*, *58*):

$$R = \begin{vmatrix} \cos\phi & 0 & \sin\phi \\ -\sin\beta\cos\phi & \cos\beta & \sin\beta\cos\phi \\ -\cos\beta\sin\phi & -\sin\beta & \cos\beta\cos\phi \end{vmatrix} \quad (3)$$

where ϕ represents the twist angle and β represents the bend at the center of the CRE/AP1 site. This rotation of a portion of a rigid body at a point using the rotational matrix ***R*** defines the movement of the FRET probe by bend and twist motions such that the new position of any point of the rigid body can be found through application of the rotation matrix as follows: choosing location coordinates (0,*d*,*l*), the twist angle (ϕ), and the bend angle (β), the matrix is multiplied by vector p_3 ($p_3 = Rp_2$) to obtain

$$p_3 = \begin{vmatrix} l \\ d \\ 0 \end{vmatrix} \quad (4)$$

where *l* is the length of the "arm" of the U-shaped probe and *d* is the distance from the center of the CRE site to the end of the base. Calculation of the distance between the two points p_1 and p_2 (R_{da}) requires the distance formula:

$$R_{da} = \sqrt{(x_1 - x_2)^2 + (y_1 - y_2)^2 + (z_1 - z_2)^2} \quad (5)$$

Applying both rotations, leaving the angles as variables, the relationship between the angles (β, ϕ) and R_{da} is obtained:

$$R_{da} = \sqrt{l^2\sin^2\phi + (d - d\cos\beta - l\sin\beta\cos\phi)^2 + (l + d\sin\beta - l\cos\beta\cos\phi)^2} \quad (6)$$

Using reasonable estimates for lengths of DNA arms, double helix geometry, and known angles for both the A_5 bulges and A_4 tracts, distances *d* and *l* are approximately 34 and 58 Å, respectively (Figure 3B). The resulting model relates R_{da} to the bend angle at the center of the CRE/AP-1 sequence. The twist, ϕ, has been well-established for FRET probe **2** and shown not to change with peptide binding. In fact, the general relationship between R_{da} and θ is relatively insensitive to small changes in ϕ (Figure 3C).

FRET Measurements. Fluorescence measurements were collected on a SPEX FluoroMax-3 spectrofluorometer equipped for steady-state conditions using a thermostated cell holder connected to a software-controlled water bath. FRET experiments were performed on the basis of previously described methods using a specially designed U-shaped duplex labeled at 5′-ends with FAM and TAMRA dyes suitable for bZIP binding (*51*, *52*). The FRET efficiency (*E*) was determined from the sensitization of the TAMRA acceptor fluorescence that normalizes the FRET signal for the acceptor quantum yield, for the concentration of the

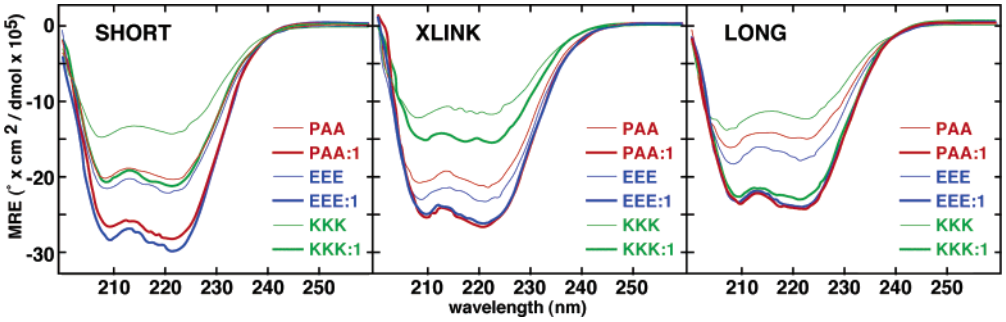

FIGURE 4: CD analysis of bZIP charge variants. Mean residual ellipticity (Θ) values for free bZIP charge variants (thin lines) and corresponding complexes with DNA duplex **1** (thick lines) were collected in buffer B (pH 7.4) as described in Materials and Methods.

duplex DNA, for bZIP-mediated donor-only or acceptor-only quenching, and for less than optimal donor−acceptor labeling. The fluorescence intensities of the emission spectra F_s(491), excited at 491 nm, where both donor (FAM) and acceptor (TAMRA) absorb energy, were fitted to the weighted sum of the two spectral components: the corrected spectrum of the donor (5′-tagged FAM) excited at 491 nm [F_d(491)] and the corrected fluorescence spectrum of the acceptor excited at 560 nm [F_a(560)]. The spectral relationships between these groups is expressed by

$$F_s(491) = AF_d(491) + \mathrm{FE}F_a(560) \quad (7)$$

where A and FE are the fitted weighting factors of the two spectral components (FAM, TAMRA) determined from least-squares fitting of eq 4 using SigmaPlot over the range of 500−700 nm. The FRET effect (FE) is the TAMRA fluorescence component of the spectrum (excited at 490 nm) normalized to the fluorescence spectrum excited at 560 nm, F_a(560). This effect is linearly dependent upon the efficiency of energy transfer, E:

$$\mathrm{FE} = E\left[\frac{\epsilon_d(491)}{\epsilon_a(560)}\right] + \frac{\epsilon_a(491)}{\epsilon_a(560)} \quad (8)$$

The ratios $\epsilon_d(491)/\epsilon_a(560)$ and $\epsilon_a(491)/\epsilon_a(560)$ were experimentally determined in all three buffer systems (A, 0.353, 0.112; B, 0.718, 0.122; C, 0.802, 0.127). Fluorescence measurements were collected in buffers A−C to confirm that results were not strongly dependent on conditions. The asymptotic FRET effect values that characterize the extent of deformation of the DNA upon 100% protein binding were determined from FRET-titration isotherms using previously described fitting procedures (*10*, *11*). The FRET efficiency, E, varies with the sixth power of the distance between the donor and acceptor, normalized to the Förster distance (R_o) that yields 50% energy transfer efficiency:

$$E = R_o^6/(R_o^6 - R_{da}^6) \quad (9)$$

Upon rearrangement, the distance between the donor and acceptor (R_{da}) can be determined using a Förster radius of R_o = 50 Å. The experimentally determined R_{da} value can be used to generate bend angle estimates using a simple geometric model approximating the shape and intrinsic twist of **2** (Figure 3).

RESULTS

Experimental Design. The bZIP domain of Gcn4p was modified by replacement of three residues distal to the basic domain to generate neutral (PAA), anionic (EEE), and cationic (KKK) charge variants (Figure 1A). Three versions of the bZIP domain ($bZIP_{SHORT}$, $bZIP_{XLINK}$, $bZIP_{LONG}$) were studied to determine which peptide scaffold provided the most stable nucleoprotein complex for analysis (Figure 1B). CRE-containing duplex **1** (Figure 1C) was used for studies of peptide folding and binding affinities. U-shaped CRE-containing duplex **2** containing terminal donor (5′-FAM) and acceptor (5′-TAMRA) fluorophores (Figure 1C) was used in FRET experiments. Other experiments involved similar DNA constructs containing AP1 sites. To examine the effects of solution conditions, three buffer systems (A, pH 6.2; B, pH 7.4; C, pH 8.3) were used in these analyses. Buffer A is a conventional FRET assay buffer with a relatively low pH (6.2) promoting favorable acceptor quantum yield. Buffer B is compared as a more physiologically relevant buffer matching binding conditions used prior to electrophoretic assays. Buffer C is the low ionic strength running buffer used in native gel electrophoretic phasing assays.

Table 1: Peptide Folding Estimates from CD at pH 7.4

		MRE[b]		helicity (%)[c]	
charge variant[a]	bZIP scaffold[a]	free	complex	free	complex
PAA	SHORT	−20300	−29000	59	89
	XLINK	−20700	−26000	61	78
	LONG	−14000	−24000	39	72
EEE	SHORT	−22100	−29500	65	90
	XLINK	−22500	−25500	67	77
	LONG	−17500	−23500	50	70
KKK	SHORT	−14000	−21400	39	63
	XLINK	−11000	−15000	29	42
	LONG	−12500	−22500	34	67

[a] See Figure 1. [b] Mean residual ellipticity of bZIP peptides free and complexed with CRE **1** in buffer B. [c] Calculated as described (*54*).

Folding of Free and DNA-Bound bZIP Charge Variants. To determine which bZIP scaffold was most stable for studies of charge variants, we characterized peptide folding using circular dichroism (CD) spectroscopy. Crystal structures of bZIP·AP1 and CRE complexes (*41*, *53*) demonstrate that the bZIP domain adopts a continuous α-helical structure when bound to DNA while the basic domain is disordered in free bZIP peptides (*59*). As such, CD is an ideal modality to monitor the transition of the basic region from random coil to a stable α-helix upon DNA binding. Far-UV CD spectra of free bZIP charge variants (10 μM) are shown in Figure 4. On the basis of mean residual ellipticity values (Θ_{222}), the helical content of each of the nine unbound bZIP charge variants was determined (Table 1). The results show a strong effect of charge on the folding stabilities of the free peptides.

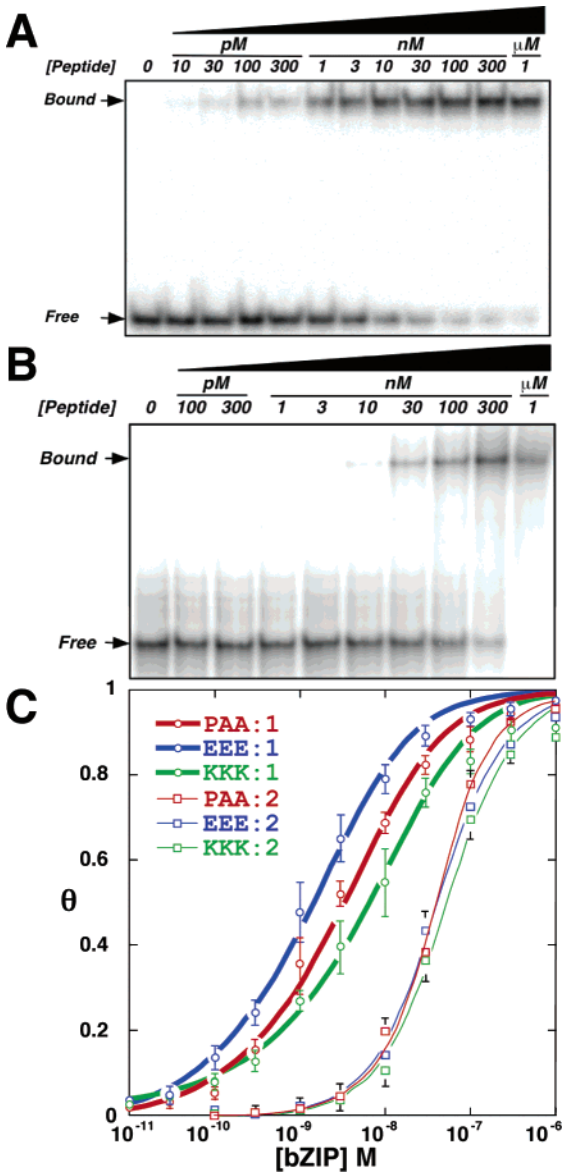

FIGURE 5: $bZIP_{LONG}$ peptide binding affinities for CRE DNA. (A) Radiolabeled CRE duplex **1** (50 pM) and increasing concentrations of $bZIP_{LONG}$ EEE peptide resolved on 12% native polyacrylamide gel in buffer B. (B) Radiolabeled U-shaped CRE duplex **2** (50 nM) and increasing concentrations of $bZIP_{LONG}$ EEE peptide resolved on 8% native polyacrylamide gel in buffer B. (C) Estimation of $bZIP_{LONG}$ binding affinities for CRE duplexes **1** (circles) and **2** (squares). Fractional DNA occupancy (θ) is plotted against the concentration of $bZIP_{LONG}$ peptide. Curve fitting is described in Materials and Methods.

Relative to the neutral charge variants (PAA), the cationic charge variants (KKK) destabilized folding, whereas the anionic variants (EEE) stabilized folding for all three bZIP scaffold constructs (Figure 1B, Table 1). Addition of cognate CRE duplex **1** to the bZIP charge variant peptides increased α-helical content in all cases (Figure 4, Table 1). As observed for free peptides, bound cationic variants (KKK) gained less α-helical structure and anionic variants (EEE) gained more α-helical structure relative to the neutral (PAA) peptides. These data show that electrostatic effects can substantially alter the folding stabilities of small peptides in the absence and presence of DNA. Placement of charged residues near the amino terminus of the bZIP peptides presumably influences stability by electrostatic interaction with the helical

Table 2: DNA Binding Affinities of $bZIP_{LONG}$ Charge Variants at pH 7.4

	K_d (nM)[b]			
DNA[a]	PAA	EEE	KKK	method
1	6.3 ± 1.5	2.7 ± 4.1	13.4 ± 3.3	PAGE
2	28.8 ± 7.7	34.9 ± 5.4	44.1 ± 10.0	PAGE
2	21.7 ± 4.9	26.4 ± 1.8	35.7 ± 21.1	FRET

[a] CRE-containing DNA duplexes (Figure 1C). [b] Mean ± standard deviation based on at least three independent measurements by electrophoretic gel mobility shift (Figure 5) for $bZIP_{LONG}$ charge variants in buffer B or fitting to FRET data as previously described (*10*, *11*).

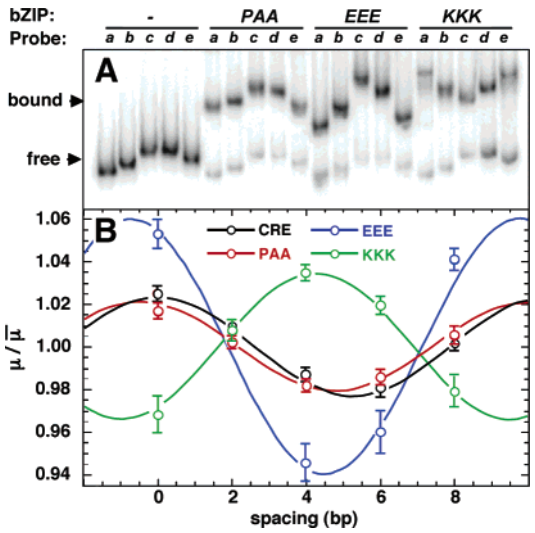

FIGURE 6: Electrophoretic phasing assay of DNA bending by $bZIP_{LONG}$ charge variants. (A) Radiolabeled phasing duplexes **a**−**e** were incubated with $bZIP_{LONG}$ peptides in buffer B (pH 7.4) and electrophoresed through 8% native polyacrylamide gel. (B) Analysis of electrophoretic phasing data for phasing duplexes **a**−**e** when free and bound to PAA, EEE, and KKK peptides. Relative mobilities of each of the five phasing duplexes in a given condition were plotted as a function of the spacing between the center of curvature in the proximal A_5 tract and the center of the CRE binding site. Normalized migration rates for each complex were fit to a phasing function to estimate the DNA bend magnitude and direction as described in Materials and Methods.

macrodipole (*60*). This interpretation is particularly supported by results obtained for the three $bZIP_{LONG}$ peptides (Figure 4, Table 1), as the charged residues in this scaffold are positioned further from the amino terminus and are predicted to interact less with the helical macrodipole. While minor stability differences are observed for free $bZIP_{LONG}$ peptides, all charge variants acquire similar α-helical content upon binding to DNA. $bZIP_{LONG}$ charge variants were selected for study in subsequent experiments.

DNA Binding Affinities of $bZIP_{LONG}$ Charge Variants. DNA binding affinities of $bZIP_{LONG}$ charge variants were obtained by electrophoretic gel mobility shift assays using CRE duplexes **1** and **2** (Figure 5). These studies determined the extent to which charge modifications affected binding affinities. Compared to $bZIP_{SHORT}$ and $bZIP_{XLINK}$ scaffolds (data not shown), the $bZIP_{LONG}$ scaffold displayed the least variation in binding affinity between neutral, anionic, and cationic variants (Table 2). In the case of CRE duplex **1**, the data in Table 2 show that the anionic charge variant has the highest affinity for the CRE DNA, followed by the neutral form and the cationic form. Unlike the other scaffolds that demonstrate significant charge-related differences in the

Table 3: Electrophoretic Estimates of CRE Bending by bZIP Charge Variants

	CRE	PAA·CRE	EEE·CRE	KKK·CRE
bend angle (deg)[a]	5.2 ± 0.3	5.7 ± 0.6	20.3 ± 1.1	12.1 ± 1.6
direction[b]	major	major	major	minor

[a] DNA bend angles were estimated as described in Materials and Methods. Mean and standard deviations reflect three independent measurements. [b] Bend direction refers to the DNA face that becomes concave, in a reference frame at the center of the CRE sequence.

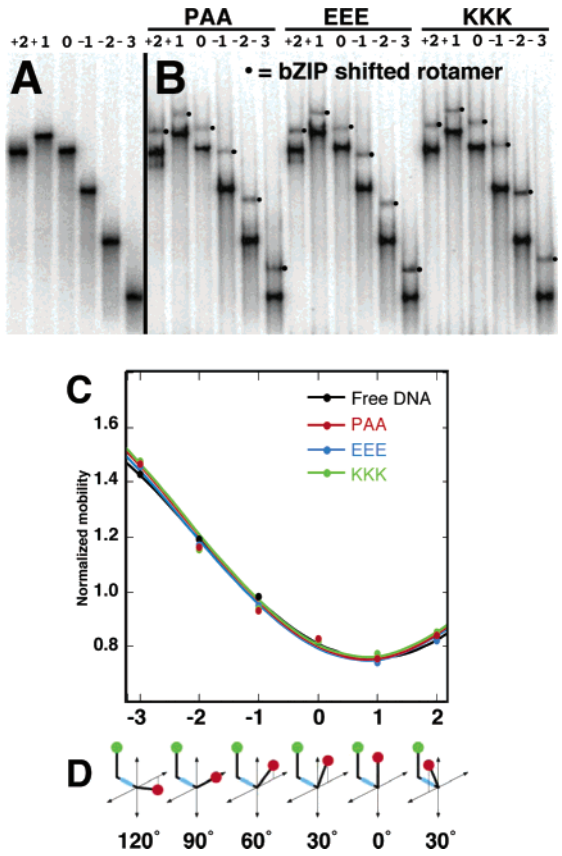

FIGURE 7: Estimation of twist in DNA probe **2**. (A) Electrophoresis of free rotamers of probe **2**. (B) Electrophoresis of rotamers bound to $bZIP_{LONG}$ charge variants. (C) Quantitation of the normalized migration of free and bZIP-bound rotamers. Data fits used to determine the minima of the cosine fitting functions are shown. The minimum of the function corresponds to planar rotamer +**1** (Figure 2). (D) Interpretation of results from electrophoretic data showing the estimated twist of each rotamer species.

peptide folding when bound to DNA (Figure 4, Table 1), similar binding affinities are observed for $bZIP_{LONG}$ peptides, in agreement with the CD results. The binding of $bZIP_{LONG}$ charge variants to a radiolabeled version of U-shaped duplex **2** was somewhat weaker than for duplex **1**. Peptide affinities from electrophoretic binding assays were in general agreement with those obtained by fitting FRET data to the appropriate binding isotherm (Table 2). These measurements established conditions for DNA bending assays.

DNA Bending by bZIP Charge Variants: Electrophoretic Phasing Analysis. We used a well-established electrophoretic DNA phasing assay that permits quantitative estimation of both the magnitude and direction of DNA bending (*43*, *45*). Phasing constructs contained a central CRE binding site variably spaced from an array of three phased A_5 tracts that serve as a curved reference. The varied spacer distance produces unique helical phasings (twist) between the phased

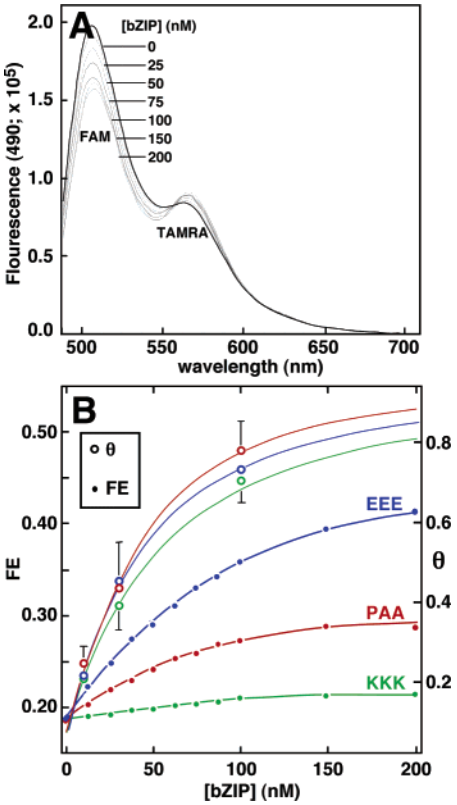

FIGURE 8: FRET effect (FE) analysis for U-shaped DNA **2** upon binding by $bZIP_{LONG}$ charge variants. (A) Example of fluorescence spectra for 50 nM DNA **2** with the indicated concentrations of $bZIP_{LONG}$ PAA in buffer B (pH 7.4). (B) FE analysis for $bZIP_{LONG}$ charge variants (filled circles) binding to U-shaped DNA **2** in buffer B. Fits to asymptotes as described in Materials and Methods were used to estimate DNA bend angles for different bZIP charge variants. Fractional saturation data (open circles) in buffer B are plotted for comparison (Figure 5).

A_5 tracts and the deformed protein binding site. When the CRE deformation is in *cis* with the phased A_5 tract, gel mobility is least, whereas a *trans* relationship between the two deflections permits greatest mobility. $bZIP_{LONG}$ charge variants were incubated with phasing probes in order to observe how charge affected apparent DNA bending (Figure 6). Results (Table 3) are consistent with our previous work (*13*−*15*). Anionic charge substitutions bend DNA by ∼15° toward the major groove, and cationic charge substitutions bend DNA by ∼15° toward the minor groove. Charge variants of $bZIP_{SHORT}$ and $bZIP_{XLINK}$ scaffolds yielded similar results, suggesting that folding stabilities of bound bZIP peptides do not affect bending in electrophoretic gels (data not shown). Similar effects were also observed in bHLH scaffolds, as the observed folding stabilities of the shorter scaffolds did not adversely affect DNA bending (*47*).

Characterization of U-Shaped DNA 2. Before applying the FAM/TAMRA conjugated form of U-shaped DNA **2** in FRET assays, we investigated the shape of this molecule using electrophoretic assays. It was important to determine the intrinsic twist (nonplanarity) of the U-shaped probe in order to properly interpret FRET changes induced by peptide binding. We generated six rotamer variants of FRET probe **2** by addition or deletion of single bp flanking the CRE site (Figures 2 and 7). Rotamers in this series differ in the degree of twist in the base of the U. To analyze the shape of these molecules by gel electrophoresis, we ligated ∼100 bp linear

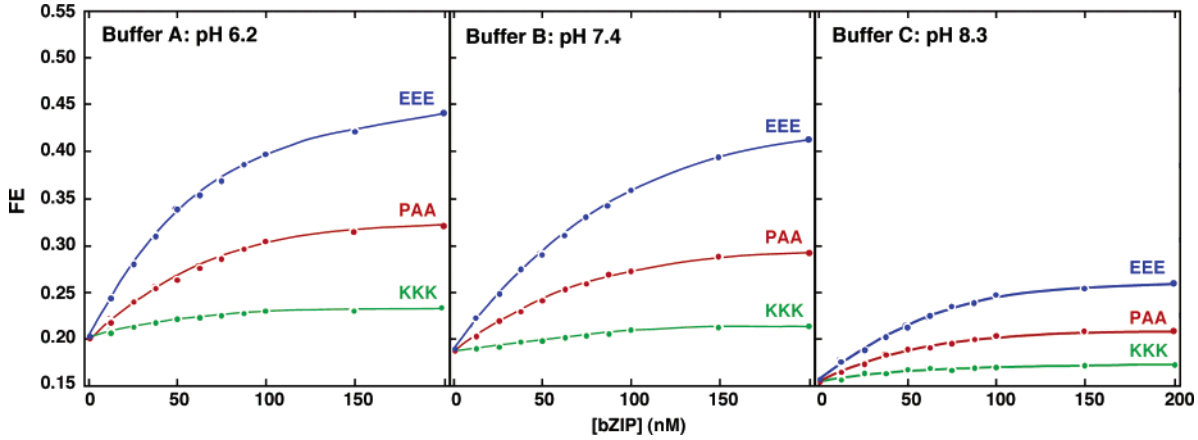

FIGURE 9: FRET effect titration curves. Asymptotic FRET effects derived from titrations of CRE-containing **2** (50 nM) with increasing concentrations of $bZIP_{LONG}$ peptide in three buffer systems: buffer A (10 mM K/HPO_4, pH 6.2, 100 mM KCl); buffer B (10 mM Na/HPO_4, pH 7.4, 137 mM NaCl, 2.7 mM KCl, 5% glycerol, 0.025% NP-40); buffer C (50 mM Tris-H_3BO_3, pH 8.3, 1 mM EDTA). bZIP charge variants are indicated by red (neutral, PAA), blue (anionic, EEE), and green (cationic, KKK).

DNA fragments to each arm to create rotamers (−**3**, −**2**, −**1**, **0**, +**1**, +**2**) and separated them on a 4.5% native acrylamide gel (Figure 7A). Addition of 100 bp arms enhanced the effect of shape on electrophoretic mobility in the native gel. These rotamers were also co-incubated and electrophoresed with $bZIP_{LONG}$ charge variants (Figure 7B). The rotamer with minimum mobility is the most nearly planar. The results (Figure 7C) indicate that probe **2** (corresponding to rotamer **0**) is intrinsically twisted by ~30° out of the plane (Figure 7D). Importantly, incubation of rotamers with $bZIP_{LONG}$ charge variants proved that none of the peptides induced additional helical twisting of the DNA (Figure 7B). On the basis of these results, a geometrical model of FRET probe **2** (without 100 bp arms) was created to extract DNA bend angle estimates from measured changes in FRET effect (FE) upon peptide binding (Figure 3). The dispositions of TAMRA and FAM fluorophores differ with respect to the DNA helix axis (*49*, *51*, *61*, *62*), introducing a small uncertainty when estimating the twist angle between the tethered fluorophores. However, DNA bend angle estimates based on our geometric model are not highly sensitive to small differences in this twist angle (Figure 3C).

DNA Bending by bZIP Charge Variants: FRET. We studied U-shaped FRET probe **2** containing either a central CRE or AP1 site (Figure 1C, flanking sequence adjusted to maintain consistent probe length) to measure effects of peptide binding and electrostatics on donor−acceptor distances by steady-state FRET (*52*). A fixed concentration (50 nM) of 5′-FAM-TAMRA-labeled duplex **2** was incubated with increasing concentrations of $bZIP_{LONG}$ charge variants under three different buffer conditions. Results for $bZIP_{LONG}$ charge variants binding to duplex **2** are shown in Figures 5B, 8, and 9 and are summarized in Table 4. In the case of buffer B (pH 7.4), unbound CRE duplex **2** is characterized by an initial FRET effect (FE) consistent with intrinsic curvature of 3.4° toward the major groove at the center of the CRE site. Neutral (PAA) charge variant binding to the CRE site in buffer A resulted in a change in the apparent DNA bend angle from 3.4° to 17.6° (net bend of 14.2° toward the major groove, i.e., toward the zipper domain of the peptide). In the case of the anionic (EEE) charge variant, the apparent bend increased by an additional 11.5° toward the major groove (29.1° of total bending). In contrast, the cationic (KKK) charge variant counteracted the DNA bend observed upon binding of the neutral charge variant, holding the DNA near its intrinsic shape (6.9° bending toward the major groove).

Table 4: FRET Estimates of CRE Bending by bZIP Charge Variants

duplex **2**	FE[b]	R_{da} (Å)[c]	bend angle (deg)[c] [relative bend angle (deg)][d]
	Buffer A (pH 6.2)[a]		
CRE	0.156 ± 0.002	69.2 ± 0.7	12.1 ± 1.0 [−12.6]
PAA_{LONG}·CRE	0.211 ± 0.001	57.9 ± 1.8	24.7 ± 2.0 [0.0]
EEE_{LONG}·CRE	0.289 ± 0.004	50.4 ± 1.2	33.1 ± 1.5 [+8.4]
KKK_{LONG}·CRE	0.171 ± 0.008	65.2 ± 1.7	16.5 ± 2.0 [−8.2]
AP1	0.154 ± 0.001	70.0 ± 0.5	11.2 ± 0.5 [−9.5]
PAA_{XLINK}·AP1	0.187 ± 0.002	61.5 ± 1.6	20.7 ± 2.0 [0.0]
EEE_{XLINK}·AP1	0.257 ± 0.006	51.8 ± 1.2	31.5 ± 1.5 [+10.8]
KKK_{XLINK}·AP1	0.158 ± 0.007	68.5 ± 1.7	12.8 ± 2.0 [−7.9]
	Buffer B (pH 7.4)[a]		
CRE	0.196 ± 0.001	71.7 ± 0.3	9.3 ± 0.5 [−14.2]
PAA_{LONG}·CRE	0.322 ± 0.011	59.0 ± 0.7	23.5 ± 1.0 [0.0]
EEE_{LONG}·CRE	0.518 ± 0.018	49.2 ± 0.8	34.4 ± 1.0 [+10.9]
KKK_{LONG}·CRE	0.223 ± 0.006	68.1 ± 1.1	13.3 ± 1.5 [−10.2]
	Buffer C (pH 8.3)[a]		
CRE	0.205 ± 0.002	72.3 ± 0.4	8.6 ± 0.5 [−14.1]
PAA_{LONG}·CRE	0.346 ± 0.002	59.7 ± 1.1	22.7 ± 1.5 [0.0]
EEE_{LONG}·CRE	0.537 ± 0.004	50.2 ± 0.7	33.3 ± 1.0 [+10.6]
KKK_{LONG}·CRE	0.232 ± 0.008	68.9 ± 1.0	12.4 ± 1.0 [−10.3]

[a] Buffer A: 100 mM KCl and 10 mM K/HPO_4, pH 6.2. Buffer B: 137 mM NaCl, 10 mM Na/HPO_4, pH 7.4, 2.7 mM KCl, 5% glycerol, and 0.025% NP-40. Buffer C: 50 mM Tris−H_3BO_3, pH 8.3, and 1 mM EDTA. [b] FRET effect (FE) values were determined by fitting to the asymptote as described in Materials and Methods. [c] Calculated from FE data as described in eqs 7−9 (Materials and Methods). Indicated uncertainties reflect standard deviations (reproducibility) and should not be interpreted as implying DNA rigidity or fluorophor restraint. In all cases, the DNA bend direction was such that the major groove face of DNA became variably concave in a reference frame at the center of the CRE or AP1 forms of DNA duplex **2** (Figure 1C). Uncertainty in the local orientation of the FAM fluorophore is estimated to affect DNA bend angle estimates by less than 20%. [d] Bend angle relative to DNA bound by the neutral bZIP charge variant. Positive values indicate bending toward the major groove at the center of the CRE/AP1 binding site.

These FRET results for $bZIP_{LONG}$ charge variants binding to the CRE site of **2** were comparable to data recorded under other binding conditions and for $bZIP_{XLINK}$ charge variants

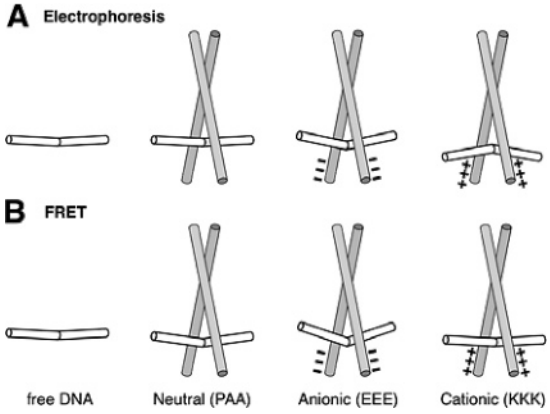

FIGURE 10: Comparison of results from electrophoretic and FRET assays of bZIP charge variants bound to the AP1 or CRE consensus site. (A) Interpretation of data from electrophoretic phasing assays. (B) Interpretation of data from FRET assays. The two assays assign slightly different shapes to the DNA in the PAA·DNA complex, but estimates of induced DNA bending relative to that complex are similar for the two methods.

binding to the AP1 site of **2** (Table 4). The data provide a coherent picture of DNA deformation by charged peptide interactions. The modest intrinsic curvature of the unoccupied CRE site is significantly enhanced (apparent DNA bend of ~14° toward the major groove) upon binding of the neutral charge variant. Placement of additional anionic amino acid residues near the minor groove face of the CRE site (EEE) increases this bend toward the major groove, as predicted by electrostatic repulsions. The placement of additional cationic residues (near the minor groove face of the CRE site) counteracts the bending observed for the neutral variant, holding DNA near its intrinsic shape. It is important to note the similarity in FRET-based DNA bend estimates for bZIP charge variants, independent of buffer conditions (buffers A, B, C), bZIP scaffold ($bZIP_{XLINK}$, $bZIP_{LONG}$), or binding site (CRE, AP1). This consistency suggests a dominant electrostatic effect in the observed DNA bending. The preservation of DNA bending in buffer B (~140 mM monovalent cation) suggests that electrostatic effects should cause DNA bending under physiological conditions.

DISCUSSION

A model summarizing the comparison between electrophoretic and FRET results is shown in Figure 10. It is striking that both electrophoretic and FRET methods estimate similar net DNA bending effects for all charge variants tested (Tables 3 and 4). Both methods suggest that 10−20° of induced DNA bending can be attributed to charge and that the directions of induced DNA deformation (relative to the neutral PAA case) are opposite for opposite charges. According to electrophoretic estimates, the shape of the DNA in the neutral PAA·DNA complex is not deformed whereas anionic and cationic bZIP charge variants bend DNA toward the major or minor grooves, respectively. FRET measurements predict the same *relative* bend magnitudes and directions for the bZIP charge variants, but with reference to a DNA bend of 17.6° toward the major groove observed for the neutral (PAA) peptide. It is not known what accounts for the difference in absolute DNA bend angle estimates for the PAA charge variant studied by electrophoretic vs FRET assays, and a contribution of the elongated peptide shape to this discrepancy cannot be ruled out. It should be noted that the FRET result reported here for the neutral (PAA) bZIP peptide binding to a CRE site compares favorably to that reported in the X-ray structure of the GCN4/CRE complex (*41*). The bend angle measured by FRET is 17.6°, and the bend in the crystal structure was 20°. The origin of this 20° bend has been argued to arise from slight local DNA unwinding and flexure to accommodate the more rigid peptide (*41*). The results of Figure 7 show that net DNA twisting does not propagate outside of the binding site.

This work supports the interpretations of previous experiments suggesting that electrostatic effects can induce modest DNA bending in predictable directions. It has been suggested that certain discrepancies might be explained by contributions of the elongated shapes or flexibilities of bound ligands such as bZIP peptides (*39*). We have recently demonstrated that comparable DNA bending effects are obtained for charge variants of both the bZIP domain of Gcn4p and the more globular bHLH domain of Pho4p in electrophoretic phasing assays (*47*). Limited data have been available to complement gel-based observations supporting the electrostatic model of DNA bending by bZIP peptides (*39*, *40*, *48*, *63*, *64*). The FRET measurements reported here independently validate our gel-based interpretations, support an electrostatic model of DNA bending, and are consistent with the notion that DNA phosphate charges contribute significantly to DNA stiffness.

When compared with the results of electrophoretic phasing assays, the present data point to DNA bending effects induced by placement of charges near DNA. Because FRET efficiency is dominated by the distance of closest approach between fluorophores, we cannot presently exclude the possibility that charge-dependent changes in DNA flexibility could also explain part or all of the observed FRET effects. This interpretation is not supported by preliminary time-resolved FRET experiments where donor decay was modeled well as a simple biexponential process in the absence or presence of bZIP peptide (data not shown). However, if the bending flexibility of free DNA is slightly enhanced upon binding to PAA, terminal fluorophores will sample shorter separations, as we observe. If the binding of KKK were to rigidify DNA [a result that would contradict a recent report (*50*)], the observed increase in average fluorophore separation could be explained. If binding of EEE were to increase DNA flexibility, the observed decrease in average fluorophore separation would be predicted. Future studies would be required to absolutely distinguish induced DNA bending and flexibility.

ACKNOWLEDGMENT

We thank T. Ellenberger and B. Müller-Hill for bZIP expression plasmids, A. Schepartz for the original pDP-AP1 phasing plasmids, M. Ramirez-Alvarado and F. Prendergast for instrument access and advice, J. Kahn for theoretical discussion and software assistance, Z. Bajzer for mathematical consultation, and J. Peterson for assistance with protein purification.

REFERENCES

1. Luger, K., Mader, A. W., Richmond, R. K., Sargent, D. F., and Richmond, T. J. (1997) Crystal structure of the nucleosome core particle at 2.8 Å resolution, *Nature 389*, 251−260.

2. Kahn, J. D., and Crothers, D. M. (1993) DNA bending in transcription initiation, *Cold Spring Harbor Symp. Quant. Biol. 58*, 115−122.
3. Goodman, S. D., and Nash, H. A. (1989) Functional replacement of a protein-induced bend in a DNA recombination site, *Nature 341*, 251−254.
4. Cantor, C., and Schimmel, P. (1980) *Biophysical Chemistry Part III: The behavior of biological molecules*, W. H. Freeman, New York.
5. Hagerman, P. J. (1988) Flexibility of DNA, *Annu. Rev. Biophys. Biophys. Chem. 17*, 265−286.
6. Manning, G. S. (1988) Three persistence lengths for a stiff polymer with an application to DNA B-Z junctions, *Biopolymers 27*, 1529−1542.
7. Parkinson, G., Wilson, C., Gunasekera, A., Ebright, Y. W., Ebright, R. E., and Berman, H. M. (1996) Structure of the CAP-DNA complex at 2.5 angstroms resolution: a complete picture of the protein-DNA interface, *J. Mol. Biol. 260*, 395−408.
8. Schultz, S. C., Shields, G. C., and Steitz, T. A. (1991) Crystal structure of a CAP-DNA complex: the DNA is bent by 90 degrees, *Science 253*, 1001−1007.
9. Manning, G. S. (2003) Is a small number of charge neutralizations sufficient to bend nucleosome core DNA onto its superhelical ramp?, *J. Am. Chem. Soc. 125*, 15087−15092.
10. Dragan, A. I., Klass, J., Read, C., Churchill, M. E., Crane-Robinson, C., and Privalov, P. L. (2003) DNA binding of a non-sequence-specific HMG-D protein is entropy driven with a substantial non-electrostatic contribution, *J. Mol. Biol. 331*, 795−813.
11. Dragan, A. I., Read, C. M., Makeyeva, E. N., Milgotina, E. I., Churchill, M. E., Crane-Robinson, C., and Privalov, P. L. (2004) DNA binding and bending by HMG boxes: energetic determinants of specificity, *J. Mol. Biol. 343*, 371−393.
12. Williams, L. D., and Maher, L. J., III (2000) Electrostatic mechanisms of DNA deformation, *Annu. Rev. Biophys. Biomol. Struct. 29*, 497−521.
13. Hardwidge, P. R., Wu, J., Williams, S. L., Parkhurst, K. M., Parkhurst, L. J., and Maher, L. J., III (2002) DNA bending by bZIP charge variants: a unified study using electrophoretic phasing and fluorescence resonance energy transfer, *Biochemistry 41*, 7732−7742.
14. Strauss, J. K., and Maher, L. J., III (1994) DNA bending by asymmetric phosphate neutralization, *Science 266*, 1829−1834.
15. Strauss-Soukup, J. K., and Maher, L. J., III (1998) Electrostatic effects in DNA bending by GCN4 mutants, *Biochemistry 37*, 1060−1066.
16. Bloomfield, V. A. (1996) DNA condensation, *Curr. Opin. Struct. Biol. 6*, 334−341.
17. Manning, G. S. (1978) The molecular theory of polyelectrolyte solutions with applications to the electrostatic properties of polynucleotides, *Q. Rev. Biophys. 11*, 179−246.
18. Manning, G. S. (2002) Electrostatic free energy of the DNA double helix in counterion condensation theory, *Biophys. Chem. 101−102*, 461−473.
19. Baumann, C., Smith, S., Bloomfield, V., and Bustamante, C. (1997) Ionic effects on the elasticity of single DNA molecules, *Proc. Natl. Acad. Sci. U.S.A. 94*, 6185−6190.
20. Halle, B., and Denisov, V. P. (1998) Water and monovalent ions in the minor groove of B-DNA oligonucleotides as seen by NMR, *Biopolymers 48*, 210−233.
21. Howerton, S. B., Sines, C. C., VanDerveer, D., and Williams, L. D. (2001) Locating monovalent cations in the grooves of B-DNA, *Biochemistry 40*, 10023−10031.
22. Hud, N. V., and Plavec, J. (2003) A unified model for the origin of DNA sequence-directed curvature, *Biopolymers 69*, 144−158.
23. Hud, N. V., and Polak, M. (2001) DNA-cation interactions: The major and minor grooves are flexible ionophores, *Curr. Opin. Struct. Biol. 11*, 293−301.
24. Hud, N. V., Sklenar, V., and Feigon, J. (1999) Localization of ammonium ions in the minor groove of DNA duplexes in solution and the origin of DNA A-tract bending, *J. Mol. Biol. 286*, 651−660.
25. McFail-Isom, L., Sines, C. C., and Williams, L. D. (1999) DNA structure: cations in charge?, *Curr. Opin. Struct. Biol. 9*, 298−304.
26. Manning, G. S., Ebralidse, K. K., Mirzabekov, A. D., and Rich, A. (1989) An estimate of the extent of folding of nucleosomal DNA by laterally asymmetric neutralization of phosphate groups, *J. Biomol. Struct. Dyn. 6*, 877−889.
27. Mirzabekov, A. D., and Rich, A. (1979) Asymmetric lateral distribution of unshielded phosphate groups in nucleosomal DNA and its role in DNA bending, *Proc. Natl. Acad. Sci. U.S.A. 76*, 1118−1121.
28. Rich, A. (1978) Localized positive charges can bend double helical nucleic acid, *FEBS Lett. 51*, 71−81.
29. Hinnebusch, A. G. (1984) Evidence for translational regulation of the activator of general amino acid control in yeast, *Proc. Natl. Acad. Sci. U.S.A. 81*, 6442−6446.
30. Hinnebusch, A. G. (1990) Involvement of an initiation factor and protein phosphorylation in translational control of GCN4 mRNA, *Trends Biochem. Sci. 15*, 148−152.
31. Suckow, M., Madan, A., Kisters-Woike, B., von Wilcken-Bergmann, B., and Muller-Hill, B. (1994) Creating new DNA binding specificities in the yeast transcriptional activator GCN4 by combining selected amino acid substitutions, *Nucleic Acids Res. 22*, 2198−2208.
32. Kerppola, T., and Curran, T. (1995) Transcription. Zen and the art of Fos and Jun, *Nature 373*, 199−200.
33. Oakley, M. G., and Dervan, P. B. (1990) Structural motif of the GCN4 DNA binding domain characterized by affinity cleaving, *Science 248*, 847−850.
34. Hagerman, P. J. (1996) Do basic region-leucine zipper proteins bend their DNA targets...does it matter?, *Proc. Natl. Acad. Sci. U.S.A. 93*, 9993−9996.
35. Kerppola, T. (1997) Comparison of DNA bending by Fos-Jun and phased A tracts by multifactorial phasing analysis, *Biochemistry 36*, 10872−10884.
36. Kerppola, T. K. (1996) Fos and Jun bend the AP-1 site: effects of probe geometry on the detection of protein-induced DNA bending, *Proc. Natl. Acad. Sci. U.S.A. 93*, 10117−10122.
37. Kerppola, T. K., and Curran, T. (1997) The transcription activation domains of Fos and Jun induce DNA bending through electrostatic interactions, *EMBO J. 16*, 2907−2916.
38. Leonard, D. A., Rajaram, N., and Kerppola, T. K. (1997) Structural basis of DNA bending and oriented heterodimer binding by the basic leucine zipper domains of Fos and Jun, *Proc. Natl. Acad. Sci. U.S.A. 94*, 4913−4918.
39. Sitlani, A., and Crothers, D. (1998) DNA-binding domains of Fos and Jun do not induce DNA curvature: an investigation with solution and gel methods, *Proc. Natl. Acad. Sci. U.S.A. 95*, 1404−1409.
40. Sitlani, A., and Crothers, D. M. (1996) Fos and jun do not bend the AP-1 recognition site, *Proc. Natl. Acad. Sci. U.S.A. 93*, 3248−3252.
41. Konig, P., and Richmond, T. J. (1993) The X-ray structure of the GCN4-bZIP bound to ATF/CREB site DNA shows the complex depends on DNA flexibility, *J. Mol. Biol. 233*, 139−154.
42. Paolella, D. N., Liu, Y., Fabian, M. A., and Schepartz, A. (1997) Electrostatic mechanism for DNA bending by bZIP proteins, *Biochemistry 36*, 10033−10038.
43. Paolella, D. N., Palmer, C. R., and Schepartz, A. (1994) DNA targets for certain bZIP proteins distinguished by an intrinsic bend, *Science 264*, 1130−1133.
44. Sloan, L. S., and Schepartz, A. (1998) Sequence determinants of the intrinsic bend in the cyclic AMP response element, *Biochemistry 37*, 7113−7118.
45. Crothers, D., and Drak, J. (1992) Global features of DNA structure by comparative gel electrophoresis, *Methods Enzymol. 212*, 46−71.
46. Koo, H. S., Drak, J., Rice, J. A., and Crothers, D. M. (1990) Determination of the extent of DNA bending by an adenine-thymine tract, *Biochemistry 29*, 4227−4234.
47. McDonald, R. J., Kahn, J. D., and Maher, L. J. (2006) DNA bending by bHLH charge variants, *Nucleic Acids Res. 34*, 4846−4856.
48. Hardwidge, P. R., Kahn, J. D., and Maher, L. J., III (2002) Dominant effect of protein charge rather than protein shape in apparent DNA bending by engineered bZIP domains, *Biochemistry 41*, 8277−8288.
49. Hillisch, A., Lorenz, M., and Diekmann, S. (2001) Recent advances in FRET: distance determination in protein-DNA complexes, *Curr. Opin. Struct. Biol. 11*, 201−207.
50. Williams, S. L., Parkhurst, L. K., and Parkhurst, L. J. (2006) Changes in DNA bending and flexing due to tethered cations detected by fluorescence resonance energy transfer, *Nucleic Acids Res. 34*, 1028−1035.

51. Lorenz, M., Hillisch, A., and Diekmann, S. (2002) Fluorescence resonance energy transfer studies of U-shaped DNA molecules, *J. Biotechnol. 82*, 197−209.
52. Dragan, A. I., Liu, Y., Makeyeva, E. N., and Privalov, P. L. (2004) DNA-binding domain of GCN4 induces bending of both the ATF/CREB and AP-1 binding sites of DNA, *Nucleic Acids Res. 32*, 5192−5197.
53. Ellenberger, T. E., Brandl, C. J., Struhl, K., and Harrison, S. C. (1992) The GCN4 basic region leucine zipper binds DNA as a dimer of uninterrupted alpha helices: crystal structure of the protein-DNA complex, *Cell 71*, 1223−1237.
54. Chen, Y. H., Yang, J. T., and Chau, K. H. (1974) Determination of the helix and beta form of proteins in aqueous solution by circular dichroism, *Biochemistry 13*, 3350−3359.
55. Pace, C. N., Vajdos, F., Fee, L., Grimsley, G., and Gray, T. (1995) How to measure and predict the molar absorption coefficient of a protein, *Protein Sci. 4*, 2411−2423.
56. Hardwidge, P. R., Zimmerman, J. M., and Maher, L. J., III (2000) Design and calibration of a semi-synthetic DNA phasing assay, *Nucleic Acids Res. 28*, E102.
57. Anton, H., and Rorres, C. (1987) *Elementary Linear Algebra with Applications*, John Wiley & Sons, New York.
58. Goldstein, H., Poole, C., and Safko, J. (2002) *Classical Mechanics*, 3rd ed., Addison Wesley, Reading, MA.
59. Weiss, M. A., Ellenberger, T., Wobbe, C. R., Lee, J. P., Harrison, S. C., and Struhl, K. (1990) Folding transition in the DNA-binding domain of GCN4 on specific binding to DNA, *Nature 347*, 575−578.
60. Munoz, V., and Serrano, L. (1995) Elucidating the folding problem of helical peptides using empirical parameters. II. Helix macrodipole effects and rational modification of the helical content of natural peptides, *J. Mol. Biol. 245*, 275−296.
61. Lorenz, M., Hillisch, A., Goodman, S. D., and Diekmann, S. (1999) Global structure similarities of intact and nicked DNA complexed with IHF measured in solution by fluorescence resonance energy transfer, *Nucleic Acids Res. 27*, 4619−4625.
62. Stuhmeier, F., Hillisch, A., Clegg, R. M., and Diekmann, S. (2000) Fluorescence energy transfer analysis of DNA structures containing several bulges and their interaction with CAP, *J. Mol. Biol. 302*, 1081−1100.
63. Kerppola, T. K., and Curran, T. (1991) DNA bending by Fos and Jun: the flexible hinge model, *Science 254*, 1210−1214.
64. Kerppola, T. K., and Curran, T. (1991) Fos-Jun heterodimers and Jun homodimers bend DNA in opposite orientations: implications for transcription factor cooperativity, *Cell 66*, 317−326.

BI061921A